Methods for Controlling Vorticity Generation at the Triple Contact Line for Wake and Drag Mitigation: An Analytical and Experimental Investigation

P. Zhang[1], A.C. DeVoria[1], and K. Mohseni[1,2]

([1]Department of Mechanical and Aerospace Engineering at University of Florida, Gainesville, FL, USA
[2]Department of Electrical and Computer Engineering at University of Florida, Gainesville, FL, USA)

ABSTRACT

In previous investigations, the moving contact line has been reported as a significant source of vorticity. In the context of ship hydrodynamics, this subject is of significant interest as vorticity generated by the countless bubbles along a ship hull likely contribute to increased drag and wake signatures. In order to understand these phenomena better and potentially increase ship efficiency and stealth, we conduct an analytical and experimental investigation of the moving contact line. Using the Stokes flow assumptions, a vorticity dipole is observed at the moving contact line. As the contact angle is increased, the vorticity flux from the corner singularity is predicted to decrease by several orders of magnitude. Experimental investigations are conducted using micro Particle Image Velocimetry (μ-PIV). Velocity fields show that increasing the contact angle using a hydrophobic coating can reduce the average vorticity near the contact line by 50%. For future mitigation of ship drag and wake signatures, we demonstrate that fluid injection near the contact line coupled with contact angle manipulation can reduce the local vorticity flux and reduce the total circulation to zero.

INTRODUCTION

In the field of naval hydrodynamics, two subjects of significant interest are ship drag and wake signatures. Due to the large size and long distances which these ships travel, ship drag can significantly impact fuel costs, range, and speed. In general, one can choose to decompose the total drag on a ship into skin friction resistance and residual resistance [Bertram (2012)]. At present, there are a wide range of works focused on reducing the skin friction resistance using methods like microbubbles [McCormick & Bhattacharyya (1973)], the Leidenfrost effect [Vakarelski et al (2011)], and hydrophobic coatings [Dong et al (2013)] among other methods [Perlin et al (2016)]. The second component of drag, residual resistance, is strongly affected by wave resistance, or the force exerted by the ship on the surrounding fluid that results in wave generation [Newman (1977), Wehausen (1973)]. Thus, the creation of a strong wake not only negatively affects ship stealth, but also indicates large wave resistance. In this paper, we examine potential solutions for reducing the strength of the wake by minimizing vorticity generation.

In studies of solid objects near a free surface, it has been observed that strong vorticity fields can lead to deformation of the interface, creation of scars and striations, and ultimately result in a persistent and easily detectable wake [Reed & Milgram (2002), Sarpkaya & Suthon (1991), Yu & Tryggvason (1990)]. As such, a reduction in vorticity generation is likely to reduce both wave resistance and wake strength. It is well established that vorticity is generated along fluid interfaces due to pressure gradients and tangential acceleration [Wu & Wu (1998), Wu et al (2006), Morton (1984), Brøns (2014), Lundgren & Koumoutsakos (1999)], however recent works have reported high concentrations of vorticity and vorticity generation in the vicinity of the triple contact line [Zhang & Mohseni (2016a), DeVoria & Mohseni (2015)]. Figure 1 is reproduced from DeVoria and Mohseni (2015) and shows the concentrated vorticity distribution and large vorticity gradients near a contact line. When we consider that the contact line length includes the ocean surface and any bubbles that are in contact with the ship hull, it is clear that vorticity generated along the total contact line length can significantly contribute to the total vorticity generated by a ship.

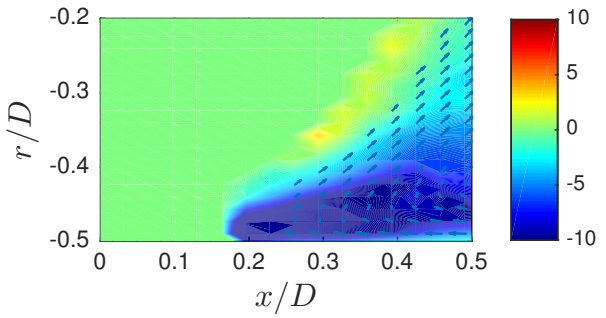

Figure 1: Experimental measurement of velocity and vorticity near a moving contact line. Reproduced with the experimental data of DeVoria and Mohseni (2015).

This is particularly true at the bow of a ship hull where waves repeatedly create an enormous number of water-air interfaces via air bubbles.

In the following sections, we begin by describing the analytical approach used to model the contact line and the experimental setup used to measure velocity. Next we consider a baseline case where it is assumed that the ship hull is hydrophilic. Based on the results we identify vortical quantities that can be minimized such that vorticity in the wake is reduced. A passive solution, via a change in contact angle, is proposed to reduce vorticity intensity and promote cross annihilation. Next, we suggest an active solution that utilizes fluid injection along the ship hull to minimize the circulation of the wake. Lastly, an experimental analysis of the effect of contact angle on vorticity generation is presented and provides convincing physical evidence of the analytical findings.

ANALYTICAL APPROACH

In this manuscript, vorticity and vorticity generation are analytically evaluated for contact line flows representative of the triple contact line along a ship hull. The analytical approach is the same as Zhang & Mohseni (2016b) and is reviewed below. To begin with, we consider a region near the triple contact line whose flow is governed by the non-dimensional incompressible Navier-Stokes equation given by

$$Re\left[\frac{\partial \boldsymbol{u}}{\partial t}+\boldsymbol{u}\cdot\nabla\boldsymbol{u}\right]=-\nabla p+\nabla^2\boldsymbol{u}. \tag{1}$$

Re is the Reynolds number, $\boldsymbol{u}$ is the velocity, t is time, and p is pressure. The Reynolds number is defined as $Re = UL/\nu$ where U is the characteristic velocity, L is the characteristic length scale, and ν is the kinematic viscosity. Note that p is the non-dimensional pressure that is scaled by $\mu U/L$ in the equation above. To simplify the problem, we limit our study to a small region near the triple contact line where the length scale, L, is small and $Re \ll 1$. Given these conditions, the Navier-Stokes equation is simplified to the Stokes equation given by

$$\nabla p = \nabla^2\boldsymbol{u}. \tag{2}$$

In addition to reducing the complexity of the governing equation, a small characteristic length scale allows us to assume that the interface is approximately straight. The simplified geometry of the triple contact line flow at small length scales is shown in the top half of figure 2 where a local polar coordinate system (r, θ) centered at the triple contact line has been defined. ϕ is the contact angle and U is the velocity of the interface relative to the solid. For the purposes of this study, fluid 1 and 2 represent water and air respectively.

While it is possible to solve equation 2, it is more convenient to solve the equivalent biharmonic stream function equation given by

$$\nabla^4\psi = 0, \tag{3}$$

whose solution was first presented by Michell (1899), and later extended by Filonenko-Borodich (1958). Based on the uniform fluid-solid boundary velocity, various terms are eliminated from the general solution and the remaining terms yield a stream function of the form

$$\begin{aligned}\psi =& rU[A\cos(\theta)+B\sin(\theta)\\ &+C\theta\cos(\theta)+D\theta\sin(\theta)].\end{aligned} \tag{4}$$

Vorticity is given by the relation $\omega = -\nabla^2\psi$ which yields the general form

$$\omega = -\frac{U[2D\cos(\theta)-2C\sin(\theta)]}{r}. \tag{5}$$

A, B, C, and D are constants determined by the boundary conditions. To simplify the analysis in the subsequent sections, we will limit our discussion to the water region, where the contact line geometry can be further simplified to a single corner as depicted in the bottom half of figure 2. In this simplified geometry, the tangential component of $\boldsymbol{u}_a$ is equal to U while the tangential component of $\boldsymbol{u}_b$ is determined by the coupled corner problem and the physical properties of water and air. From the results of Huh & Scriven (1971), the tangential component of $\boldsymbol{u}_b$ is dictated by the water-air viscosity ratio, $R_\mu = \mu_1/\mu_2 \approx 55.2$.

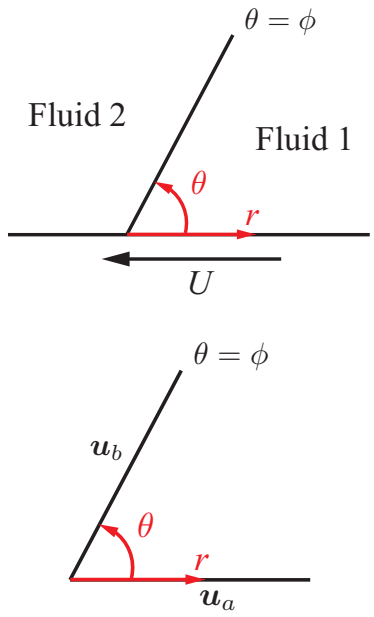

Figure 2: (*top*) Schematic of triple contact line flow where $Re \ll 1$. A polar coordinate system (r, θ) is defined with its origin centered at the contact point. (*bottom*) Schematic of corner flow at length scales where $Re \ll 1$.

EXPERIMENTAL SETUP

The contact line is investigated experimentally using a translating water-air interface in a glass tube actuated via a syringe pump (see DeVoria and Mohseni (2015) for more details). The velocity field is measured with μ-PIV; for details refer to Santiago et al (1998). The tube diameter is $D = 1.5$ mm and the flow is magnified with a 10× microscope objective. This yields a spatial resolution of $(\Delta x, \Delta y) = (0.043D, 0.021D) \approx (64\mu\text{m}, 32\mu\text{m})$ for the μ-DPIV. Hence, the measurements are within the 'hydrodynamic regime,' where the interface shape is affected by viscous effects [Snoeijer & Andreotti (2013)], but are not on the scale of the Stokes flow approximation. White-light microscope images are used to identify the water-air interface and compute the apparent contact angle and interface shape. Two cases are investigated: an uncoated and coated (hydrophobic Fluoropel PFC601AC) solid surface.

UNMODIFIED CONTACT ANGLE

To establish a baseline case, we consider an idealized water-air interface moving relative to a ship hull with a dynamic contact angle of 75° and scaled velocity $u_r(r, \theta = 0) = -1$. The velocity along the water-air interface determined by the coupled corner solution is $u_r(r, \theta = 0) = 0.6$. At present, we assume that there is zero mass flux across both interfaces and thus $u_\theta(r, \theta = 0) = u_\theta(r, \theta = 75°) = 0$. The water velocity and vorticity fields given by these boundary conditions are shown in figure 3.

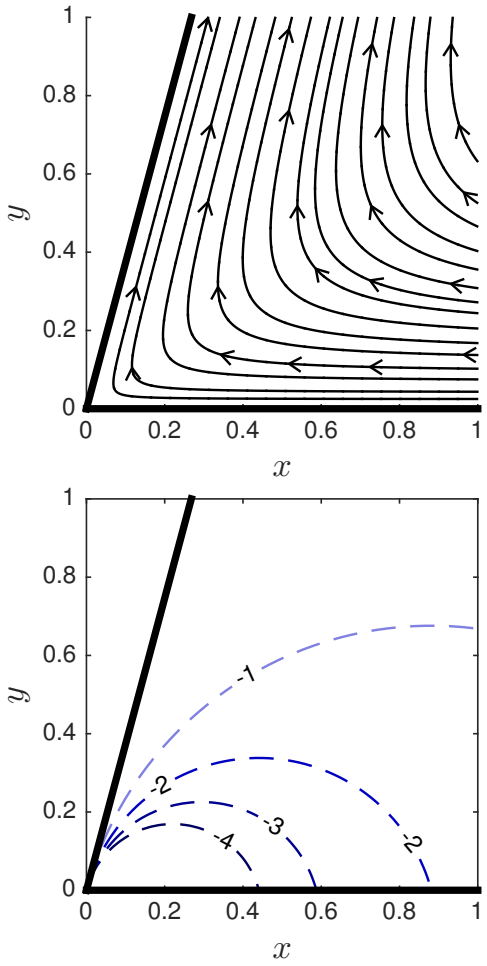

Figure 3: (*top*) Velocity and (*bottom*) vorticity field of water near the triple contact line. Boundary conditions are given by $\phi = 75°$, $u_r(r, \theta = 0) = -1$, $u_r(r, \theta = 75) = 0.6$, $u_\theta(r, \theta = 0) = u_\theta(r, \theta = 75°) = 0$. Solid lines (—) denote the boundaries of the corner and the dashed lines (- -) denote contours of constant vorticity.

As discussed by Zhang & Mohseni (2016a,b), the vorticity distribution takes the form of a dipole whose field can be written as

$$\omega = \frac{\alpha}{r}\cos(\theta - \beta), \tag{6}$$

where α is the dipole strength and β is the dipole

orientation. These quantities are functions of contact angle and boundary velocities only as shown by Zhang & Mohseni (2016a). The boundary conditions determine the strength and orientation of the dipole with respect to the corner. In the case shown above, the dipole is oriented so that the water within the corner is characterized by negative vorticity, however it is possible for both positive and negative vorticity to exist, see DeVoria and Mohseni (2015).

To quantify the effect of the contact line on the drag and wake, we will use the dipole strength and circulation defined by

$$\alpha = 2U\sqrt{C^2 + D^2}, \tag{7}$$

$$\Gamma = \oint_{\partial S} \boldsymbol{u} \cdot d\boldsymbol{\ell} = \iint_S \omega dS$$
$$= \int_0^1 \int_0^\phi \alpha \cos(\theta - \beta) dr d\theta. \tag{8}$$

The contour ∂S is defined as the wedge with unit radius that encloses the fluid inside the corner. A stronger dipole strength indicates large shear stresses along the boundary which, multiplied by contact line length along a ship hull, can contribute significantly to drag. For the remainder of the discussion, the dipole strength is used as a measure of the potential wake minimization, as a decrease in its magnitude is correlated to a decrease in total circulation, local skin friction, and vorticity generation near and at the the contact line. The circulation near the contact line will be used as an estimate of the amount of vorticity that may be convected downstream into the wake. As vorticity has been linked to persistent wakes, minimizing the total vorticity that can be convected downstream may decrease wake signatures. Moreover, even if such vorticity is not convected to the wake, the energy required for its generation will decrease ship range and speed. Note that zero circulation does not necessarily mean that there is no vorticity, but rather that the positive and negative vorticity are present in equal quantities and may cross annihilate.

To minimize drag and persistent wakes, we propose two methods for minimizing dipole strength and circulation. First, we suggest contact angle manipulation, via hydrophobic [Feng et al (2002)] coating or electrowetting [Baird et al (2007), Mugele & Baret (2005)], to decrease the dipole strength. Second, we propose implementation of a uniform wall normal velocity along a ship hull to reduce the total circulation. For reference, the baseline case shown above is characterized by $\alpha = 1.83$ and $\Gamma = -1.36$. The relative scale of these quantities will become clear in the following sections.

MODIFICATION OF CONTACT ANGLE

The contact angle, and its effect on fluid drag has been well studied in microscopic applications [Mugele & Baret (2005), Ou et al (2004)]. However, its application to large scale problems in corrosive environments, like that of a ship in the ocean, has not been as prevalent. In an experimental study by Dong et al (2013), it was reported that increasing the contact angle to 159.7°, induced by a superhydrophobic coating, yields a significant reduction in drag. To further understand the effects of contact angle, the analytic methodology established above is used to conduct a parametric study. Figure 4 shows the predicted dipole strength and circulation magnitude for various contact angles.

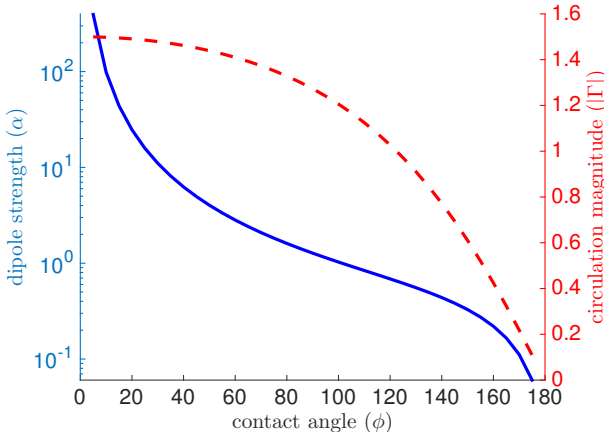

Figure 4: Strength of the vorticity dipole (α) and total circulation (Γ) with respect to changes in contact angle (ϕ). The solid blue line represents the dipole strength and the dashed red line represents the magnitude of the circulation.

At small contact angles, $\phi < 45°$, incremental changes in contact angle result in a significant decrease in the dipole strength and moderate changes in total circulation. As contact angle increases, dipole strength continues to decrease, albeit at a slower rate. On the other hand, circulation exhibits large changes as contact angle increases. These results indicate that an increase in the contact angle will reduce the dipole strength and thus the drag. Therefore, we consider the modified contact line flow, with a focus on vorticity, where the contact angle is increased from 75° to 150°. The resulting velocity field and vorticity field in the vicinity of the contact line is shown in figure 5. Qualitatively, the flow does not experience as much turning and has a smoother transition through the corner. This results in a dipole strength of 0.33 and

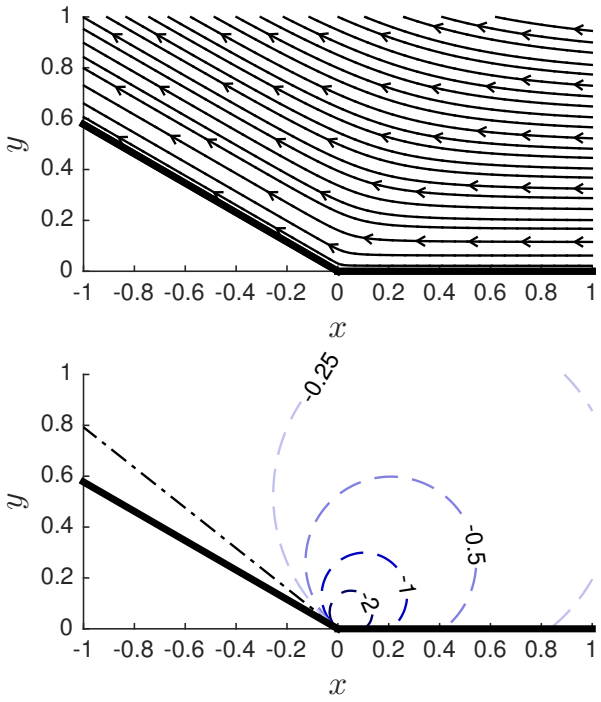

Figure 5: (*top*) Velocity and (*bottom*) vorticity field of water near the triple contact line. Boundary conditions are given by $\phi = 150°$, $u_r(r, \theta = 0) = -1$, $u_r(r, \theta = 150) = 0.9$, $u_\theta(r, \theta = 0) = u_\theta(r, \theta = 150°) = 0$. Solid lines (—) denote the boundaries of the corner, dashed lines (– –) denote contours of constant vorticity, and the dash-dotted lines (– · –) denote the vorticity contour of magnitude 0.

circulation of -0.61, where a two-fold increase in contact angle predicts a 82% reduction in dipole strength and 55% reduction in circulation magnitude. From figure 5, it can be seen that the reduction in circulation is primarily due to a lower average vorticity. However, the vorticity is still primarily of one sign. In ship applications, this vorticity is convected downstream and can result in the creation of undesirable persistent wakes.

While the contact angle in the above example was defined, it has been shown in numerous experiments that this angle is achievable for water using passive methods like hydrophobic coating [Feng et al (2002)] or surface patterning [Truesdell et al (2006)]. An active method like electrowetting [Baird et al (2007), Mugele & Baret (2005)] is also capable of modifying the contact angle using electric fields and may prove to be a more robust option given the harsh ocean environment.

In general, the analysis above is valid for any contact line. In naval hydrodynamics, it is expected to affect the air bubbles that move across a ship hull. The top half of figure 6 depicts an air bubble moving relative to an unmodified solid surface where the vorticity generated at both contact points is primarily of the same sign. Modifying the surface via electrowetting or hydrophobic coatings will increase the advancing and receding contact angle, ϕ_A and ϕ_R relative to the water, resulting in a reduction of vorticity intensity along the entire contact line. The cumulative effect of thousands of bubbles is likely to have a significant impact the total vorticity within the wake.

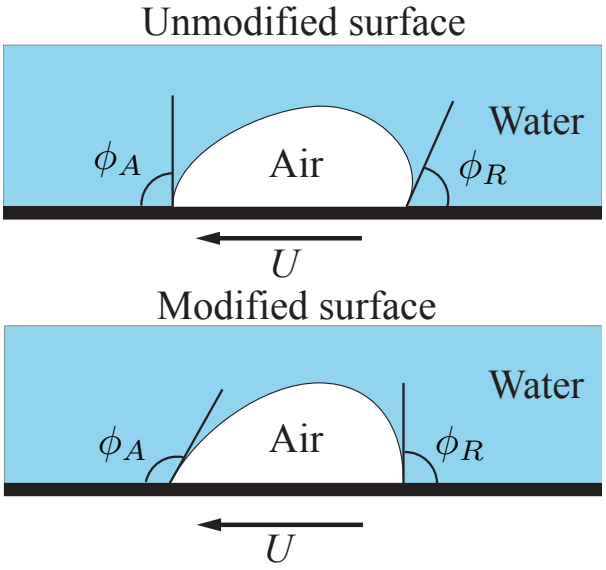

Figure 6: (*top*) Air bubble moving relative to an unmodified solid surface. (*bottom*) Air bubble moving relative to a hydrophobic surface. The result is larger advancing, ϕ_A, and receding, ϕ_R, contact angles, which are relative to the water.

Based on the analysis above, the optimal contact angle appears to be at angles greater than 160° where both α and Γ are minimized. Unfortunately, manufacturing and maintaining a surface with a contact angle greater than 160° is a challenging task. Therefore we consider other methods of vorticity control that are effective at more moderate hydrophobic angles.

MODIFICATION OF WALL NORMAL VELOCITY

In Zhang & Mohseni (2016), it was determined that vorticity dipoles are not only characteristic of moving contact line flows, but also of corner flows with wall normal velocity. At small scales near the contact line, where the Stokes equations govern the flow and

superposition is valid, there is the opportunity to add wall normal velocity to reduce the total circulation. Based on the configuration of a ship, control of the water-air interface $\theta = \phi$ is highly unlikely. It is far more reasonable to consider control of the boundary normal velocity along the ship hull. Therefore, we only consider solutions that can be controlled via u_θ at $\theta = 0$.

In figure 7, an independent solution driven by uniform wall normal velocity, $u_\theta(r, \theta = 0) = 0.5$, is shown. Due to limited control of the flow boundary conditions, the orientation of the dipole is fixed given the contact angle and zero mass flux through the water-air interface. The magnitude of the wall normal velocity at $\theta = 0$ is only capable of changing the strength of the dipole. In this example, the magnitude of u_θ has been chosen so that the strength of this dipole is equal to the dipole created by wall tangential velocity only. The combined flow is shown in figure 8.

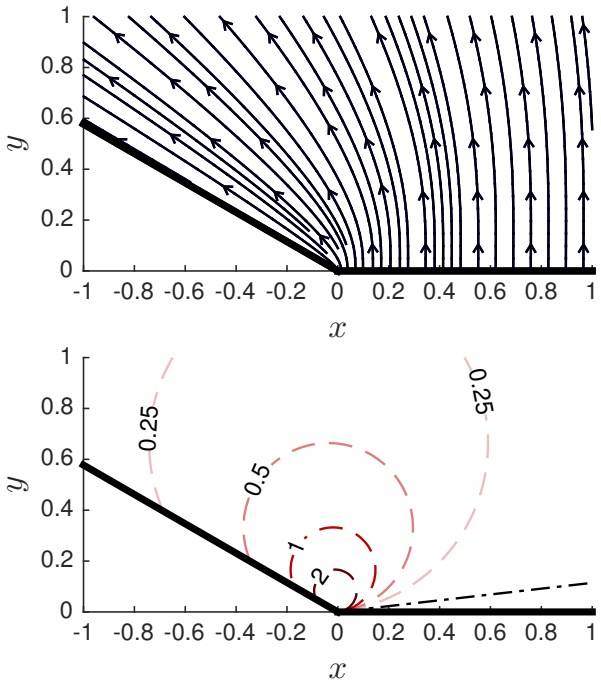

Figure 7: (*top*) Velocity and (*bottom*) vorticity field of water near the triple contact line. Boundary conditions are given by $\phi = 150°$, $u_r(r, \theta = 0) = u_r(r, \theta = 0) = 0$, $u_\theta(r, \theta = 0) = 0.5$, and $u_\theta(r, \theta = 150°) = 0$.

Figure 8 represents the net effect of the two proposed methodologies for reducing drag and wake generating vorticity. First the contact angle was increased from 75° to 150° which resulted in a decrease in vorticity dipole strength and total circulation. Here, we have added a wall normal velocity along the boundary whose magnitude is one half the velocity of the interface relative to the the ship hull. The result of applying a wall normal velocity is a vorticity dipole with strength $\alpha = 0.26$ and a balanced amount of positive and negative vorticity, giving approximately zero total circulation. The addition of wall normal velocity reduced the vorticity intensity along the wall and near the contact line in addition to creating a significantly more balanced vorticity field that may cross annihilate when confined to the small regions near the contact line.

While the example provided was conducted for a contact angle of 150°, the same method can be applied for any contact angle. However, as contact angle decreases, the the ratio of the wall normal velocity to wall tangential velocity will increase. As this ratio increases above 1, it may become increasingly difficult to implement. Thus these methods are most effective when applied in conjunction.

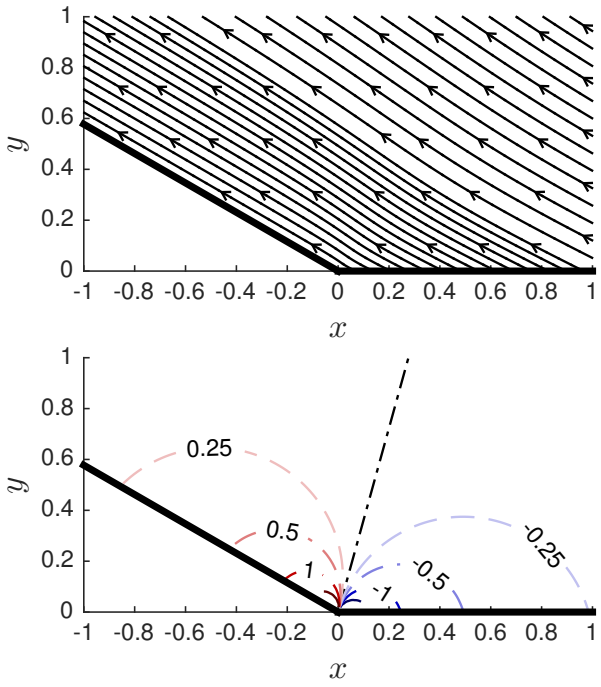

Figure 8: (*top*) Velocity and (*bottom*) vorticity field of water near the triple contact line. Boundary conditions are given by $\phi = 150°$, $u_r(r, \theta = 0) = -1$, $u_r(r, \theta = 150°) = 0.9$, $u_\theta(r, \theta = 0) = 0.5$, and $u_\theta(r, \theta = 150°) = 0$.

Note that the interface velocity relative to the ship hull, U, is not necessarily the velocity of the ship. Experimental measurements of bubble interaction with a ship hull is sparse due to the measurement difficulty. Furthermore, bubbles cannot be replicated in scaled models as there is limited control of bubble

size. However, we can estimate that the velocity of an air bubble along the ship hull will be small relative to the velocity of the ship. This is based off the assumption that the bubble lies inside the ship boundary layer and the length scale of the bubble is significantly smaller than the thickness of the boundary layer.

EXPERIMENTAL RESULTS

Although the experiments are in the 'hydrodynamic regime,' they are not capable of resolving the nanometric or Stokesian regime with as much detail as the analytical results presented above. The Reynolds number based on the tube diameter is $Re_D \approx 1.25$ and the resolution is such that the local Reynolds number is less than 0.1 for only a portion of the image. However, the main purpose of the experiments is to see if the vorticity dipole character of the flow very near the contact line is observable on the larger macroscopic flow length scale. Such experimental evidence would give credence to our concept of the triple contact line as a source of vorticity.

First, we show the angle of the water-air interface (i.e. meniscus angle) relative to the tube wall as a function of distance from the wall in figure 9. The position is determined from the white-light microscope images of the dynamic interfaces. The apparent contact angle, θ_{ap} is found by extrapolating the fitted interface curve to the tube wall. As expected, the coating has a major effect on the interface shape and the apparent contact angle increases from $\theta_{\text{ap}} \approx 32^\circ$ to 68°.

The asymptotic solution proposed by Voinov (1976) estimates the contact angle to have a logarithmic dependence on distance from the wall as

$$\theta(y) \approx [9Ca \log(y/c)]^{1/3}, \qquad (9)$$

where Ca is the capillary number and c is a constant that corresponds to the length scale at which molecular forces are dominant and regularize the viscous singularity at the triple contact point [Snoeijer & Andreotti (2013)]. It should be noted that for receding contact lines, such as the current experiments, the above equation is not likely to be valid at large distances from the contact line. Nonetheless, we can interpret the effect of increasing the meniscus and apparent contact angles by noting that the uncoated case has a more prominent logarithmic dependence. Hence, for this case, the parameter c could be inferred to be larger than the coated case, and consequently increases the region in which molecular forces

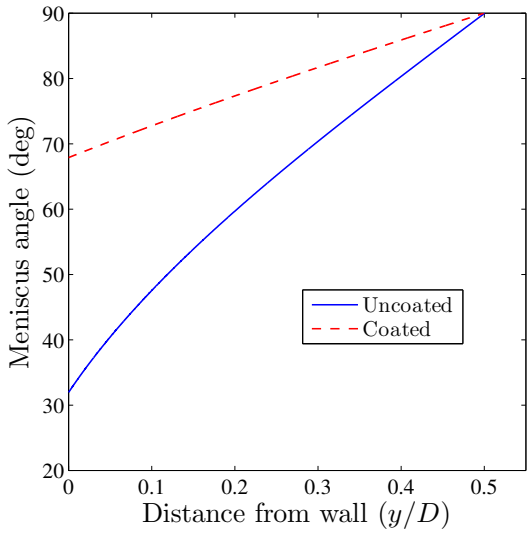

Figure 9: The meniscus angle as a function of distance from the tube wall. The values at $y/D = 0$ represent the apparent contact angle and $y/D = 1/2$ is the center-line of the tube where $\theta = 90^\circ$.

are dominant. In terms of the vorticity dipole, the increase of c would correspond to an increase of α and thus vorticity generation and circulation.

Now we consider how the macroscopic flow field changes from an increase in contact angle, and if these reflect a possible source of vorticity at the contact line. Figure 10 shows velocity vectors, vorticity, and the water-air interface location for the uncoated and coated cases. Inside a wedge of radius $r/D < 0.15$ the local Reynolds number is less than 0.125 and the vorticity is of one sign, which is qualitatively consistent with the analytic solutions presented previously. Although the measurements do not have the resolution to observe the singular vorticity distribution at microscopic/molecular distances from the contact line (see equation 6), we can still observe a significant increase in the vorticity magnitude as the contact line is approached. This again implies that the dipole at the origin is in fact generating vorticity.

However, the overall vorticity field at larger distances from the contact line displays different behaviors from the limiting Stokes solution. For example, there is significant opposite sign vorticity (positive in this case) appearing along the water-air interface farther from the contact line, which has been observed previously [DeVoria & Mohseni (2015)]. Figure 10 suggests the intensity of both signs of vorticity are affected by the interface curvature. To quantify this, we wish to consider a quantity that characterizes

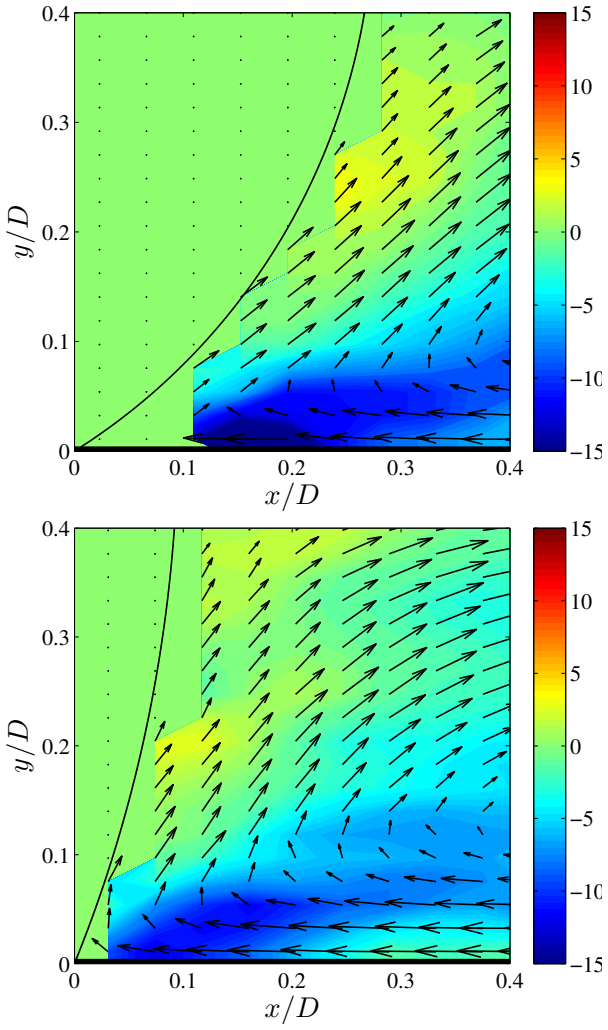

Figure 10: Experimentally measured velocity vectors overlaid on the vorticity field. The thin black curve represents the water-air interface. (*top*) Uncoated and (*bottom*) coated tube wall. Note the change in the apparent contact angle.

the vorticity, but also accounts for the different sizes of the spatial areas occupied by the vorticity. Therefore, we compute the circulation magnitude divided by the integration area, which is equivalent to the average vorticity magnitude, say $\bar{\omega}$, in that region. This is done for positive, negative, and total vorticity. Figure 11 plots $\bar{\omega}_+$, $\bar{\omega}_-$, and $\bar{\omega}$ against $R = \sqrt{A}$ where A is the integration area and R may be interpreted as the distance from the contact line. Note that the Stokes flow solution predicts $\bar{\omega}$ of the form r^{-1}, which is consistent with the experiment data in figure 11 for the total and negative vorticity magnitudes. The uncoated case, characterized by a smaller contact angle, has considerably larger average vorticity with approximately a 50% increase in $\bar{\omega}$ and $\bar{\omega}_-$ near the contact line. For $\bar{\omega}_+$, the magnitudes for both cases are much lower since positive vorticity only appears from the water-air interface. Initially $\bar{\omega}_+$ is similar between the two cases, but by $R/D > 0.2$ the positive vorticity for the uncoated case increases above that of the coated case. This is because the boundary-layer-like vorticity on the water-air interface is more intense due to the stronger curvature for the uncoated case. The true $\bar{\omega}_+$ magnitudes near the interface are likely to be larger, however the DPIV data cannot fully resolve that vorticity and is 'stair-cased'. While this positive vorticity can result in some annihilation, this process could induce large-scale mixing. Under these circumstances, mixing could become unstable leading to a turbulent wake signature. For example, more air bubbles could be entrained at the water-air interface thus making the wake more easily identifiable.

CONCLUSION

In this study, the vorticity near moving contact lines was investigated using analytic and experimental methods. It was observed that for an unmodified, hydrophilic surface, the vorticity intensity is large and mostly of one sign. Left uncontrolled, this may lead to the generation of persistent wakes indicative of significant wave resistance. To address these issues, we proposed a passive and active method for minimizing the vorticity dipole intensity and circulation near the contact line. Passively, the vorticity near the contact line can be controlled by hydrophobic coatings or electrowetting. Analytic predictions showed that under ideal circumstances, the vorticity intensity may decrease by as much as 82% with a 55% reduction in circulation. Experimentally, the contact angle was altered via a hydrophobic coating and resulted in significant changes to the large-scale flow features, including an apparent contact angle change of 32° to 68°. In particular, increasing the experimental contact angle reduced the average vorticity near the contact angle by 50%. These trends agree with the analytical model of Stokes flow and provide evidence that a vorticity dipole located at the contact line acts as a source of vorticity. Furthermore, opposite sign vorticity is generated along the water-air interface due to the interface curvature, which may have implications on turbulent mixing of the ship wake. In addition to contact angle manipulation, the total circulation near the contact line can be controlled via fluid injection along the water-solid boundary. In the example discussed in this paper, the total circulation was reduced to zero, however this can be adjusted to

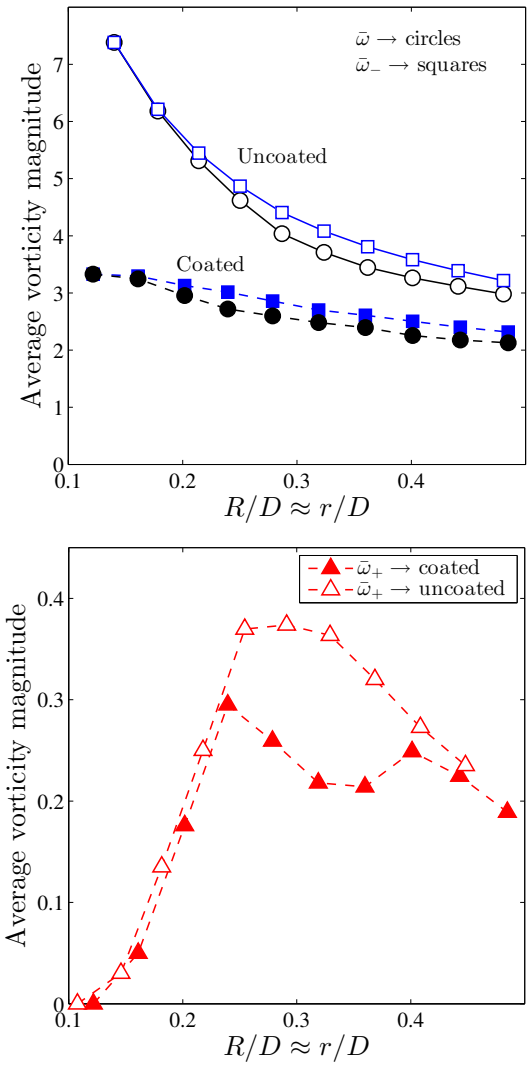

Figure 11: Average vorticity magnitudes for the uncoated (open symbols) and coated (solid symbols) cases as functions of distance from the contact line. (*top*) Total (circles) and negative average vorticity (squares). (*bottom*) Positive average vorticity.

a wide range of values given sufficient control over the wall normal velocity. Future investigations will seek to gather more detailed experimental data for verification of the analytic model and implement experimental testing of the proposed control methods.

REFERENCES

Baird, E., Young, P., and Mohseni, K., "Electrostatic Force Calculation for an EWOD-actuated Droplet," Microfluidics and Nanofluidics, Vol. 3, No. 6, 2007, pp. 635-644.

Bertram, V., Practical Ship Hydrodynamics, Elsevier, 2012.

Brøns, M., Thompson, M. C., Leweke, T., and Hourigan, K., "Vorticity Generation and Conservation for Two-dimensional Interface and Boundaries, Journal of Fluid Mechanics, Vol. 758, 2014, pp. 63-93.

DeVoria, A. C., Mohseni, K., "Droplets in an Axisymmetric microtube: Effects of Aspect ratio and fluid interfaces," Physics of Fluids, Vol. 27, No. 1, 2015, pp. 1-18.

Dong, H., Cheng, M., Zhang, Y., Wei, H., and Shi, F., "Extraordinary Drag-reducing Effect of a Superhydrophobic Coating on a Macroscopic Model Ship at High Speed," Journal of Materials Chemistry A, Vol. 1, No. 19, 2013, pp. 5886-5891.

Feng, L., Li, S., Li, Y., Li, H., Zhang, L., Zhai, J., Song, Y., Liu, B., Jiang, L., and Zhu, D., "Superhydrophobic Surfaces: From natural to artificial," Advanced Materials, Vol. 14, No. 24, 2002, pp. 1857-1860.

Filonenko-Borodich, M., Theory of Elasticity, University Press of the Pacific, Moscow, 1958.

Huh, C. and Scriven, L. E., "Hydrodynamic Model of Steady Movement of a solid/liquid/fluid Contact line," Journal of Colloid and Interface Science, Vol. 35, No. 1, 1971, pp. 85-101.

Li, F. and Mugele, F., "How to Make Sticky Surfaces Slippery: Contact Angle Hysteresis in Electrowetting with Alternating Voltage," Applied Physics Letters, Vol. 92, No. 24, 2008, pp. 1-3.

Lundgren, T. and Koumoutsakos, P., " On the Generation of Vorticity at a Free Surface," Journal of Fluid Mechanics, Vol. 382, 1999, pp. 351-366.

McCormick, M. E. and Bhattacharyya, R., "Drag Reduction of a Submersible Hull by Electrolysis," Naval Engineers Journal, Vol. 85, No. 2, 1973, pp. 11-16.

Michell, J. H., " On the Direct Determination of Stress in an Elastic Solid, with Application to the Theory of Plates," Proceedings of the London Mathematical Society, Vol. 1, No. 1, 1899, pp. 100-124.

Morton, B. R., "The Generation and Decay of Vorticity,"

Geophysical and Astrophysical Fluid Dynamics, Vol. 28, No. 3-4, 1984, pp. 277-308.

Mugele, J., and Baret, J. C., "Electrowetting: From Basics to Applications," Journal of Physics: Condensed Matter, Vol. 17, No. 28, 2005, pp. 705-774.

Newman, J. N., Marine Hydrodynamics, MIT Press, 1977.

Ou, J., Perot, B., and Rothstein, J., "Laminar Drag reduction in microchannels using Ultrahydrophobic Surfaces," Physics of Fluids, Vol. 16, No. 12, 2004, pp.4635-4643.

Perlin, M., Dowling, D. R., and Ceccio, S. L., "Freeman Scholar Review: Passive and Active Skin Friction Drag Reduction in Turbulent Boundary Layers," Journal of Fluids Engineering, 2016.

Reed, A. M. and Milgram, J. H., "Ship wakes and their radar images," Annual Review of Fluid Mechanics, vol. 34, No. 1, 2002, pp. 469-502.

Santiago, J. G., Wereley, S. T., Meinhart, C. D., and Adrian, R. J., "A Particle image velocimetry system for microfluidics. Experiments in Fluids, Vol. 25, 1998, pp. 316-319.

Sarpkaya, T. and Suthon, P., "Interaction of a vortex couple with a free surface," Experiments in Fluids, Vol. 11, No. 4, 1991, pp. 205-217.

Snoeijer, J. H. and Andreotti, B., "Moving Contact Lines: Scales, Regimes, and Dynamical Transitions," Annual Review of Fluid Mechanics, Vol. 45, 2013, pp. 269-292.

Truesdell, R., Mammoli, A., Vorobieff, P., van Swol, F., and Brinker, J. C., "Drag Reduction on a Patterned Superhydrophobic Surface," Physical Review Letters, Vol. 97, 2006, pp. 044504.

Vakarelski, I. U., Marston, J. O., Chan, D. Y., and Thoroddsen, S. T., "Drag Reduction by Leidenfrost vapor layers," Physical Review Letters, Vol. 106, No. 121, 2011, pp. 214501.

Voinov, O. V., "Hydrodynamics of wetting," Fluid Dynamics, Vol. 11, No. 5, 1976, pp. 714-721.

Wehausen, J. V., "The Wave Resistance of Ships," Advances in Applied Mechanics, Vol. 13, 1973, pp. 93-245.

Wu, J-Z., Ma, H-Y., and Zhou, M-D., Vorticity and Vortex Dynamics, Springer, 2006.

Wu, J-Z. and Wu, J. M., "Boundary Vorticity Dynamics since Lighthill's 1963 Article: Review and Development," Theoretical and Computational Fluid Dynamics, Vol. 10, No. 1-4, 1998, pp. 459-474.

Yu, D. and Tryggvason, G., "The Free Surface Signature of Unsteady, Two-dimensional Vortex Flows," Journal of Fluid Mechanics, Vol. 218, 1990, pp. 547-572.

Zhang, P. and Mohseni, K., " Dipole Vorticity Sources at Sharp Corners along a Fluid Interface," Proceedings of the AIAA Aerospace Sciences Meeting, San Diego, CA, USA, January 4-8 2016.

Zhang, P. and Mohseni, K., "Sources of Vorticity at Corner Singularities along Fluid Interfaces," *under review at* Journal of Fluid Mechanics, 2016.

Discussion

Matthew J. Ringuette,
Associate Professor,
University of Buffalo.

1. Would there be a benefit to a spatially-varying wall-normal velocity (blowing) along the wall– one that is local, at the expected scale of the bubbles?

2. Could the Authors provide a sample white-light microscope image of the dynamic interface, perhaps for the presentation? For the moving interface, does any motion blur play a role in creating uncertainty for determining the contact angle?

3. Is there any value in somehow relating the curvature of the air/water interface to the vorticity, e.g. via a nondimensional parameter, to compare the uncoated and coated wall cases?

4. Regarding the fluid injection to control the vorticity and circulation, there are a few future discussion items that can be considered. Would this be done as "blowing" via discrete water jets, or do the Authors envision some other method? If so, is there a minimum required jet diameter, e.g. on the order of the average bubble size? Is this practical/necessary along the entire hull? Or, perhaps it can be done only in key sections near the front of the ship, where it might be most effective?

Author's reply

1. With a spatially varying wall-normal velocity, it would be possible to reduce the vorticity intensity slightly more. However, when we consider that this analysis applies to the contact line of every bubble in contact with a ship hull, implementation of a spatially varying wall normal velocity quickly becomes impractical.

2. The white light image of the droplet is shown in figure 12. The red line shows the fitted interface used to determine the contact angle and no motion blur is observed.

3. The effect of interface curvature on vorticity generation has been discussed by Brøns (2014) and Lundgren & Koumoutsakos (1999). In general, there are multiple factors that influence the shape of the interface so that curvature cannot be predicted based solely on the hydrophobicity of the channel. Thus any characterization of the vorticity with respect to the curvature is unlikely to applicable to other problems.

4. At present the envisioned method would be discrete jets. It is not necessary or practical to implement these jets along the entire hull. Rather it would be most effective to place these jets strategically near the ship bow where the local flow is the most bubbly.

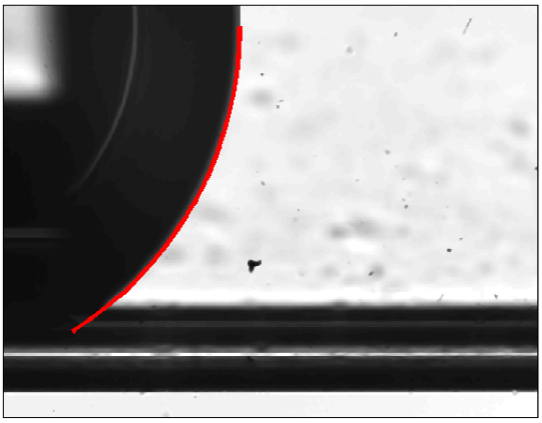

Figure 12: White light image of uncoated case. The red line is interface obtained from fitting a polar curve $r(\theta)$ to the pixels identified from an edge finding.